European Journal of Pharmaceutical Sciences 187 (2023) 106489

Contents lists available at ScienceDirect

European Journal of Pharmaceutical Sciences

journal homepage: www.elsevier.com/locate/ejps

Aerosolized sulfated hyaluronan derivatives prolong the survival of K18 ACE2 mice infected with a lethal dose of SARS-CoV-2

Mauro Pavan [a,*], Chiara D. Fanti [a], Alba Di Lucia [a], Elena Canato [b], Laura Acquasaliente [b], Fabio Sonvico [c], Jennifer Delgado [d], Amberlee Hicks [e], Jordi B. Torrelles [e], Viraj Kulkarni [d], Varun Dwivedi [d], Anna M. Zanellato [a], Devis Galesso [a], Gianfranco Pasut [b], Francesca Buttini [c], Luis Martinez-Sobrido [d], Cristian Guarise [a]

[a] Fidia Farmaceutici SpA, via Ponte della Fabbrica 3/A, 35031 Abano Terme, Italy
[b] Department of Pharmaceutical and Pharmacological Sciences, University of Padova, Via F. Marzolo 5, 35131, Padova, Italy
[c] Food and Drug Department, University of Parma, Parco Area delle Scienze 27a, 43124 Parma, Italy
[d] Disease Intervention and Prevention Program, Texas Biomedical Research Institute, San Antonio, TX 78227, USA
[e] Population Health and Host-Pathogens Interactions Programs, Texas Biomedical Research Institute, San Antonio, TX 78227, USA

ARTICLE INFO

Keywords:
SARS-CoV-2
sHA
K18-hACE2 mice, Aerosol delivery

ABSTRACT

Despite several vaccines that are currently approved for human use to control the pandemic caused by severe acute respiratory syndrome coronavirus 2 (SARS-CoV-2), there is an urgent medical need for therapeutic and prophylactic options. SARS-CoV-2 binding and entry in human cells involves interactions of its spike (S) protein with several host cell surface factors, including heparan sulfate proteoglycans (HSPGs), transmembrane protease serine 2 (TMPRSS2), and angiotensin-converting enzyme 2 (ACE2). In this paper we investigated the potential of sulphated Hyaluronic Acid (sHA), a HSPG mimicking polymer, to inhibit the binding of SARS-CoV-2 S protein to human ACE2 receptor. After the assessment of different sulfation degree of sHA backbone, a series of sHA functionalized with different hydrophobic side chains were synthesized and screened. The compound showing the highest binding affinity to the viral S protein was further characterized by surface plasmon resonance (SPR) towards ACE2 and viral S protein binding domain. Selected compounds were formulated as solutions for nebulization and, after being characterized in terms of aerosolization performance and droplet size distribution, their efficacy was assessed *in vivo* using the K18 human (h)ACE2 transgenic mouse model of SARS-CoV-2 infection.

1. Introduction

Severe acute respiratory syndrome coronavirus 2 (SARS-CoV-2) has caused the global coronavirus disease 2019 (COVID-19) pandemic infecting more than 600 million people and causing more than 6 million deaths by September 2022 (WHO Coronavirus (COVID-19) Dashboard). Most of SARS-CoV-2 infected people are asymptomatic or manifest mild symptoms (Chu et al., 2020), while a small subset develops acute respiratory distress syndrome (ARDS), characterized by difficult breathing and low blood oxygen levels, which may result into respiratory failure (Tay et al., 2020; Lamers and Haagmans, 2022). Much of the SARS-CoV-2 mortality has been associated with a cytokine storm syndrome in people admitted to hospital with severe COVID-19 (Tay et al., 2020). Several vaccines are currently approved for human use to control the pandemic (Tregoning, Flight, Highham, Wang, & Pierce, 2021); however, virus mutations lead to vaccine breakthroughs (Farinholt et al., 2021) and therefore, there is an urgent medical need for alternative therapeutic and prophylactic options, such as antivirals that could be beneficial and alleviate symptoms and prevent hospitalizations by lessening the replication of SARS-CoV-2 and/or inhibiting viral attachment on the host cell surface.

SARS-CoV-2 transmits from an infected host either by droplets, direct physical contact, indirect contact (fomites) and aerosols (Inglis and Mathee, 2021). Primary sites of viral infection are the upper and lower respiratory airways from where it could become systemic (Trypsteen et al., 2020). SARS-CoV-2 binding and entry in human cells involves

* Corresponding author.
E-mail address: mpavan@fidiapharma.it (M. Pavan).

https://doi.org/10.1016/j.ejps.2023.106489
Received 21 March 2023; Received in revised form 19 May 2023; Accepted 6 June 2023
Available online 11 June 2023

interactions of its receptor binding spike (S) protein with several host cell surface factors, including heparan sulfate proteoglycans (HSPGs), transmembrane protease serine 2 (TMPRSS2), and angiotensin-converting enzyme 2 (ACE2) (Wu et al., 2020). HSPGs encompasses a group of glycoproteins composed of unbranched negatively charged heparan sulfate (HS) chains covalently attached to a core protein. HS chains are composed of alternating D-glucuronic Acid (GlcA) and N-acetyl Glucosamine (GlcN) disaccharide units that can be variably sulfated (De Pasquale, Quiccione, Tafuri, Avallone, and Pavone, 2021). In mammals, most cell types express HSPGs. Due to HSPGs heavily sulfated HS chains, these present a global negative charge that can interact electrostatically with the basic residues of viral surface glycoproteins or capsid proteins (Cagno et al., 2019). HSPG binding is exploited by several viruses including, but not limited to, coronavirus (CoV), Human Immunodeficiency Virus (HIV), Herpes Simplex Virus (HSV), and Rhinovirus (Cagno et al., 2019). Natural (Mycroft-West et al., 2020; Paiardi et al., 2022) and synthetic sulfated (Nie et al., 2021; Bertini et al., 2022) polysaccharides have been shown to bind to SARS-CoV-2 S protein (Kwon et al., 2020) and to inhibit cell entry of other viruses (Bianculli et al., 2021). Sulfated hyaluronan (sHA), a chemical derivative of hyaluronic acid (HA), is structurally similar to HS as both polysaccharides are composed of GlcA and GlcN but differs in sugar linkages and sulfation patterns (Hintze et al., 2012). Recently, sHA has been shown to effectively inhibit SARS-CoV-2 infection in Caco-2 cells (Möller et al., 2022). To the same group of glycosamicoglycan (GAG) belongs heparin, which due to its peculiar structure possesses anticoagulant activity contrary to sHA (Guarise et al., 2018). Further, inhaled heparin is reported to significantly improve breathing capability in COVID-19 patients (Erelel et al., 2021). Additionally, Toelzer et al. demonstrated that *in vitro* binding of the S protein of SARS-CoV-2 with linoleic acid leads to a configuration change in the virus that make it less prone to ACE2 recognition and binding (Toelzer et al., 2020). Indeed, unsaturated fatty acids can inhibit SARS-CoV-2 S protein interaction with ACE2 and TMPRSS2 and viral infection of human cells (Goc et al., 2021).

All these studies show that engaging the S protein of SARS-CoV-2 using different "decoy" approaches can be a useful strategy to block host cell attachment and interaction with ACE2. Aerosolized delivery of these molecules is critical as the drug directly and rapidly reaches the target site, *i.e.* the upper and lower respiratory airways, so these become readily available to encounter the virus which could not be achieved when administered via oral or parenteral routes.

The goal of this study was to investigate the potential of sHA to inhibit the binding of SARS-CoV-2 to the human (h)ACE2 receptor and whether the presence of a hydrophobic side moiety would lock this binding. After screening of different sulfation degree of sHA backbone, a series of sHA functionalized with a range of hydrophobic side chains, including saturated and unsaturated fatty amines, were synthesized and tested for inhibitory binding efficacy of S protein of SARS-CoV-2 to the hACE2 receptor. The water-soluble compounds selected for the highest binding affinity to the viral S protein, were further characterized by surface plasmon resonance (SPR) against ACE2 and viral S protein Receptor Binding Domain (RBD). The active compounds were formulated as solutions for nebulization and aerosols produced by a jet-nebulizer were characterized in terms of respirability and droplet size distribution. Finally, the efficacy of these compounds to protect against SARS-CoV-2 infection was assessed *in vivo* using transgenic mice expressing hACE2 from the human cytokeratin 18 promoter (K18), a well validated mouse model of SARS-CoV-2 infection (Oladunni et al., 2020).

2. Materials and methods

2.1. Materials

Hyaluronic acid (HA) sodium salt (HA Na; Mw 200 kDa) and HA tetrabutylammonium salt (HA TBA) were provided by Fidia Farmaceutici S.p.A. (PD, IT). Ultrapure water (UPW) was generated using a water treatment apparatus by Sartorius (IT). Adipogen (CA; US) supplied the kit SARS-CoV-2 Inhibitor Screening Kit (#AG-48B-0001) and SARS-CoV-2 Spike Protein S1 RBD (#CHI-B232004;); Clinic Sciences (RM; IT) supplied Sensolyte 390 ACE2 Activity Assay kits Fluorimetric (Catalog# AS-72,086); BPS Bioscience, Inc. (CA; US) supplied TMPRSS2 Fluorigenic Assay Kit (96-well), (#78,083); Fisher Scientific (IT) provided Biacore sensor chip CM5. All other reagents were supplied by Sigma (IT), unless specified otherwise, and used without further purification.

2.2. Synthesis and characterization of sHA and sHA derivatives

sHA with a degree of sulfation (DS) of 1.3 and 2.1 [expressed as the average number of sulfate groups per disaccharide repeating unit (r.u.)], were synthesized from HA as reported (Guarise et al., 2018). The DS was determined by measurements of the sulfur content (Table 1) using an inductively coupled plasma–optical emission spectrometer (ICP-OES) (Perkin Elmer, IT) operating at 181.975 nm. The MW was measured by GPC-TDA Viscotek analysis (Pavan et al., 2016). sHA derivatives were synthesized from the sHA (DS=2.1) TBA salt and obtained as a freeze-dried powder from the sHA Na salt after cation exchange resin (DOWEX M-31). For synthesis of the sHA derivatives, 1.5 g (1.3 mmol; 1 eq: sHA r.u.) of sHA TBA salt was dissolved at 40 °C in 90 ml of DMSO, and then 0.04 mL (0.4 eq.) of methanesulfonic acid was added. Then, 40 mg (0.19 eq.) of 1,1-carbonyldiimidazole (CDI) was added slowly and after 10 min, followed by 0.9 eq. of the amine specific for each derivative. Fifteen different derivatives were synthetized (Table 1). After 16 h at 40 °C in each reactor, a saturated aqueous NaCl solution (5 ml) was added, and the product was recovered by adding 200 ml of ethanol (EtOH) into the solution and filtering the precipitate. The powder was then washed several times using a mixture of EtOH and water to remove the free hydrophobic amine and finally it was dried in an oven at 38 °C. Following this procedure, approximately 0.9 g of each sHA derivative was obtained. The degree of derivatization was measured by ^{1}H NMR (Bruker; D_2O, 400 MHz) (see Supporting Information), and the results are tabulated in Table 1.

2.3. SARS-CoV-2 inhibitor screening assay

The sHA derivatives were solubilized in DPBS at 8 mg/ml and diluted to the final concentration of 533.4 μg/ml; 35.6 μg/ml; 2.4 μg/ml and 1.2 μg/ml, in the ELISA buffer provided in the SARS-CoV-2 inhibitor screening kit (Adipogen, US). The plate was coated (overnight at 4 °C) with 100 μl of the monomeric S protein (1 μg/ml). After the washing step, 50 μl of each sample was added to each well. After 20 min at room temperature, 50 μl of biotinylated hACE2 receptor (1 μg/ml) were added to each well and incubated for 1 h at 37 °C. After the washing step, streptavidin-HRP were added to each well and substrate development was conducted by the addition of TMB. After the addition of the stop solution the optical density (O.D.) was measured at 450 nm. The 50% inhibitory concentration (IC_{50}) value for each sHA derivative was determined fitting with a sigmoidal plot the normalized sHA derivative activity *vs.* its concentration. Two different experiments were performed, both in triplicate ($n = 6$ for each sample). The assay was repeated with the three inhibitors (**#d, #e** and **#f**, Table 1) following the same procedure described above but using the trimeric S protein (concentration 0.4 μg/ml) for the coating of the plate. The trimeric S protein trimer (0.086 mg/ml) was kindly provided by Prof. Angelini (University of Venice, IT).

2.4. ACE2 activity assay

ACE2 (His-Tag Human Recombinant, NSO Cells; Merck, IT) was diluted to 5 ng/ml in the assay buffer. ACE2 enzyme (80 μl at 5 ng/ml) was added to each well. Then, 20 μl of the three inhibitors (**#d, #e** and

Table 1
List of sHA derivatives (*e.g.*, sHA-CO—NH-hydrophobic moiety; sHA backbone with a DS of 2.1) with the derivatization degree (analyzed via ^{1}H NMR) and the inhibitory activity of the binding between the ACE2 receptor and the monomeric or trimeric SARS-CoV-2 Spike protein. Data are expressed as mean ± S.D.; $n = 6$ (values, 2 experiments in triplicate). The last two column indicate the inhibition activity *vs.* ACE2 and TMPRSS2 protease binding ($n = 3$; -: not tested).

Name	Scaffold	Hydophobic moiety *-R	Deriv. degree	IC_{50} (μg/mL) *vs* Spike protein		IC_{50} (μg/mL)	
			% mol/mol	monomer	trimer	*vs* ACE2	*vs* TMPRSS2
a	sHA-CO-*	–	–	2587 ± 1472	5722 ± 2311	–	–
b	sHA-CO-*	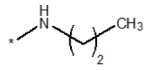	10.3 ± 1.6	> 266	–	–	–
c	sHA-CO-*	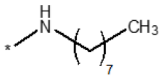	9.1 ± 1.0	> 266	–	–	–
d	sHA-CO-*	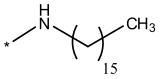	7.8 ± 0.4	4.9 ± 4.0	121.0 ± 81.9	> 800	> 800
e	sHA-CO-*	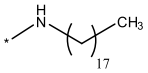	10.2 ± 0.9	3.7 ± 2.9	142.8 ± 96.6	> 800	> 800
f	sHA-CO-*	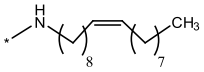	10.3 ± 1.0	5.7 ± 5.1	84.9 ± 57.4	> 800	> 800
g	sHA-CO-*	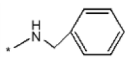	12.2 ± 1.2	> 266	–	–	–
h	sHA-CO-*	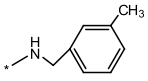	10.3 ± 1.7	> 266	–	–	–
i	sHA-CO-*	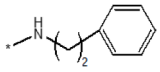	9.9 ± 1.0	> 266	–	–	–
j	sHA-CO-*	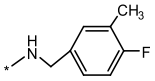	10.2 ± 1.5	> 266	–	–	–
k	sHA-CO-*	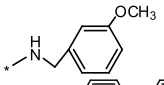	9.8 ± 1.0	213.9 ± 33.6	–	–	–
l	sHA-CO-*	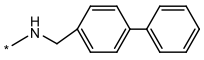	9.3 ± 0.9	> 266	–	–	–
m	sHA-CO-*	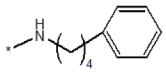	11.8 ± 0.6	> 266	–	–	–
n	sHA-CO-*	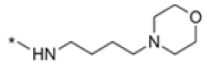	5.5 ± 0.5	> 266	–	–	–
o	sHA-CO-*	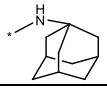	6.1 ± 0.6	194.8 ± 22.8	–	–	–

#f, Table 1) were added to each well with the ACE2 enzyme, at a final concentration of 0.8 mg/ml. The assay buffer was used as negative control, the inhibitor (DX600, CAS: 478,188–26–0) provided with the kit was used as positive control. The plate was incubated at 37 °C for 5 min. Mca/Dnp ACE2 substrate (100 μl) was added to each well and the fluorescence (exitation: 330 nm/emission: 390 nm) was recorded with the Infinite M200Pro TECAN ($n = 3$).

2.5. TMPRSS2 fluorogenic assay

TMPRSS2 enzyme (30 μl at 0.5 ng/μL) and 10 μl of the three inhibitors (**#d, #e** and **#f**, Table 1) were added to wells at the final concentration of 0.8 mg/ml. The assay buffer was used as negative control, while the inhibitor Camostat (provided with the kit from BPS Biosciences, US) was used as positive control. The 96-well plate was incubated for 30 min at room temperature. The fluorogenic TMPRSS2 substrate (20 μl) was added to each well and after 10 min at room temperature, the fluorescence (excitation: 383 nm/emission: 455 nm) was recorded with the Infinite M200Pro TECAN ($n = 3$).

2.6. Cytotoxicity assay

The cytotoxicity was measured according to the ISO 10,993–5:2009, using BALB/3T3 clone A31 mouse fibroblasts (ATCC® CCL-163), as previously described (Guarise et al., 2018). The inhibitors tested (sHA DS2.1 and **#f**, Table 1) were sterilized by filtration at 0.2 μm ($n = 4$) and evaluated against untreated cells (negative control) and 0.5 mM Sodium Dodecyl Sulfate (SDS; positive control).

2.7. Surface plasmon resonance (SPR) binding affinity to hACE2 or viral S RBD protein

SPR measurements were carried out at 25 °C on a dual flow cell Biacore-X100 instrument (GE Healthcare). Two different carboxymethylated CM5 sensor chips were first derivatized at pH 4.5 with viral monomeric S protein RBD and hACE2, respectively. Aliquots (60 μl) of tested sample solutions at increasing concentrations were injected over the S protein and hACE2 sensor chips in PBS pH 7.0 at a flow rate of 30 μl/min, with a contact time of 60 s. Each binding curve was subtracted for the corresponding baseline obtained on the reference flow cell and accounting for non-specific binding. The dissociation constant (K_d)

relative to the binding of each tested sample to either immobilized spike protein or hACE2 was obtained as a fitting parameter by plotting the value of the response units at the steady state (RU_{eq}) as function of tested sample concentration and interpolating the data points with Eq. (1):

$$RU_{eq} = RU_{max} \times \frac{[L]}{K_d + [L]} \quad (1)$$

where L is the concentration of tested sample, and RU_{eq} and RU_{max} are the response units, measured at the steady state, at intermediate and saturating [L]. The binding data were analyzed using the BIAevaluation software.

2.8. Formulation and sterilization of drug product

sHA (DS 2.1) was dissolved at the final concentration of 40 mg/ml in citrate buffer 6 mM (pH 3.5, 4.5 or 5.5) or in PBS 10 mM buffer (pH 7.0); samples were stored in glass vial. sHA (DS 2.1) in PBS buffer was sterilized by 0.2 μm filtration (Minisart CA 0.2 μm; Sartorius, IT) or by autoclave. Compound **#f** was dissolved at the final concentration of 10 mg/mL in PBS 10 mM buffer pH 7.0.

2.9. Stability study

All the formulated sHA (DS 2.1) at 40 mg/ml or **#f** at 10 mg/ml solutions were stored at 55 °C for 45 days. At time zero and after 45 days, samples were analyzed for Mw GPC-TDA Viscotek analysis (Pavan et al., 2016). Free sulfate was extracted by diluting samples in ethanol and measured by means of HPLC-UV (Agilent, IT), using the following conditions: Benzenesulfonic acid 1 g/l and sodium tetraborate 0.5 g/l pH 8.8 mobile phase; 2.0 ml/min flow isocratic for 12 min; detector set at 250 nm; Dionex IonPac AS14A 4.0 × 250 mm column; 40 μl injection. Negative peak from sulfate ion was quantified against standard calibration curve prepared with Na_2SO_4. Residual bound sulfate was calculated by subtracting free sulfate from total sulfate (ICP-OES; see 2.2).

2.10. Nebulization assay

The evaluation of the nebulization of sHA (DS 2.1) at 40 mg/ml and **#f** at 10 mg/mL solutions was done by *in vitro* aerosol performance. The two solutions described above were nebulized using an Air Family Evolution (Pikdare S.P.A, Italy) compressor nebulizer assembled with Pic Acti-Fast Pro ampoule. Drug Delivery Rate (DDR) and total Drug Delivered (DD) values were determined following the test described in USP43 "Products for nebulization- Characterization Tests", monograph 1061 (Ceschan et al., 2022). Briefly, the mouthpiece of the nebulizer was connected to a breathing simulator (VCS S.r.l, Parma, Italy), which created a cycle of 15 breaths and a suction volume of 500 ml, the standard breathing pattern defined for adults. A glass filter fiber (1 μm, diameter 76 mm, Pall Corporation) was inserted in the filter holder. The ampoule was filled with 3 ml of sHA (DS 2.1) at 40 mg/ml or **#f** at 10 mg/ml solution, the pump was switched on and at the beginning of an inhalation cycle, the nebulizer was activated. After 1 min, the filter was removed and collected for the DDR determination. The filter was substituted with a new one until the end of the nebulization for the total DD determination.

The aerodynamic particle size distribution of the nebulized aerosol was conducted as reported by USP43 "Products for nebulization- Characterization Tests" USP-NF43, monograph 1061 (Ceschan et al., 2022) using a Next Generation Impactor (NGI). The NGI (Coplay Scientific Limited, UK) was connected to a sampling vacuum pump (Coplay Scientific Limited, UK) with a continuous aspiration flow rate set at 15 l/min. The ampoule was filled with 3 mL of sHA (DS 2.1) solution at 40 mg/ml or **#f** at 10 mg/ml solution. The nebulizer was activated for a sampling time of 4 min. The amount of drug substance on the IP, stages 1–7 and micro-orifice collector (MOC) was quantitatively collected.

All the samples were collected with water for the quantification using a Blyscan sGAG Assay Kit (Biocolor Ltd, UK), a quantitative dye-binding assay for the *in vitro* analysis of the sulfated glycosaminoglycans (sGAG). The kit allowed, following a reaction between the dye-reagent and the sulfate derivative, to obtain a color of the analyzed solution with an intensity proportional to the concentration of the sulfate derivative. The samples were detected with Tecan Spark multimode plate reader 10 M (Tecan Trading AG, Switzerland) colorimeter. Experiments were carried out in triplicates. DDR and total DD, MMAD and Respirable Fraction values were calculated using Microsoft Excel.

2.11. Ethics statement

In vivo experiments in K18 hACE2 female mice with SARS-CoV-2 WA-1/US 2020 strain were conducted in animal biosafety level 3 (ABSL3) laboratories at Texas Biomedical Research Institute (Texas Biomed). Studies were approved under Texas Biomed Biosafety (BSC20–004), and by the Texas Biomedical Institutional Animal Care and Use Committee (IACUC, 1718 MU16). Texas Biomedical Research Institute facilities and programs of the Vivarium and Division of Laboratory Animal Medicine are fully accredited by the Association for the Assessment and Accreditation of Laboratory Animal Care, International (AAALAC) and are in compliance with state law, federal statute and NIH policy (such as the National Research Council's Guide for the Care and Use of Laboratory Animals).

2.12. Mice

Five weeks old female K18 hACE2 transgenic mice (stock no: 034,860; $n = 52$) were purchased from The Jackson Laboratory. Mice were housed in micro-isolator cages in the ABSL3, provided with sterile water and chow *ad libitum*, and acclimatized for one week prior to experimental manipulation. All mice were healthy and were ear punched for identification at the start of the experiment.

2.13. Cell culture

Vero E6 cells obtained from the American Type Culture Collection (ATCC, CRL 1586) were cultured in Dulbecco's Modified Eagle Medium (DMEM) supplemented with 10% heat inactivated fetal bovine serum (FBS), penicillin (P; 100 IU/ml), streptomycin (S; 100 μg/ml) and L-glutamine (G; 292 μg/ml) at 37 °C in a 5% CO_2 atmosphere incubator.

2.14. SARS-CoV-2 preparation

SARS-CoV-2 WA-1/US 2020 strain (Genbank accession MT020880) was obtained from the Biodefense and Emerging Infections Research Resources Repository (BEI Resources, NR-52,281). This SARS-CoV-2 WA-1/US 2020 strain was isolated from an oropharyngeal swab from a middle-age patient with a respiratory illness in January 2020 in the state of Washington, United States. The virus stock received from BEI Resources was a passage (P4) stock. BEI Resources P4 stock was used to generate a master P5 seed stock. The P5 stock was further used to generate a P6 working stock. Both P5 and P6 SARS-CoV-2 WA-1/US 2020 stocks were generated by infecting Vero E6 cells at low multiplicity of infection (MOI, 0.01) for 72 h. At 72 h post-infection, cell culture supernatants were collected, clarified, aliquoted, and stored at −80 °C. A standard plaque assay (plaque forming units, PFU/ml) in Vero E6 cells was used to titrate P6 viral stock (2.5×10^6 PFU/ml). Both P5 seed and P6 working stocks were sequenced, using next generation sequencing, and were identical to the virus obtained from BEI Resources.

2.15. Mass dosing system

For aerosol delivery of the test articles, we used a mass dosing system

from Data Science International (DSI; St. Paul, MN, USA). The Mass Dosing chamber is a rectangular acrylic box with a flexible design that accommodates various types of aerosol and bias flow sources. A port on the lid is designed for an Aerogen Aeroneb® nebulizer. A port on one end accepts 22 mm aerosol fittings. Five Luer fittings are provided for other aerosol configurations, bias flow sources, and exhaust. The chamber volume is 36.6 L (17.5 × 11.75×10.88 inches). The nebulizer is a micropump device, that can output at a flow rate of 100 μl/min and has a maximum capacity of 10 ml, 2.5 to 4 μm particle size production. The setting used for this study was 10% duty; 1 LPM (0.1 ml/min).

2.16. Treatment regimen and infection

On study day 0, mice were sedated with isoflurane and challenged intranasally (I.N.) with 1×10^4 PFU/mouse of SARS-CoV-2 WA-1/US 2020 in a total volume of 50 μl. Mice in group 1 (mock infection) were similarly inoculated with PBS in a final volume of 50 μl. Prior to infection, individual mouse body weight was recorded. Starting at study day 0 (1–2 h after infection), PBS or sHA or compound **#f** was administered via aerosol route twice daily for 5 consecutive days in a 6–8 hour interval. Mass dosing system was optimized to run 3.1- 3.3 ml solution in 35 min. The corresponding dose of sHA and #f delivered were 2.4 mg and 0.6 mg per mouse per dose respectively. The doses were determined using the equation as reported by Johnson et al. (Alexander et al., 2008; Wolff, 2015):

$$DD = C \times RMV \times D$$

DD= delivered dose; C= concentration of substance in air (mg/L); RMV=volume of air inhaled in one minute; *D*=duration of exposure (min).

RMV was calculated by the equation:

$$RMV(L/min) = 0.608 \times \text{body weight of mice}(kg)^{0.852}$$

The average body weight of mice in the study was 0.0164 kg

Mice in the mock infection control group received aerosolized PBS twice in a 6–8 h interval, at day 0.

2.17. Sample processing

Mice (n = 4/group) were euthanized via inhalational of CO_2 followed by cervical dislocation on days 2 and 4 post infection for viral load determination. Lung (all lobes except the right caudal lobe) and nasal turbinate were harvested and homogenized in 1 ml of sterile PBS using a Precellys tissue homogenizer (Bertin Instruments, Rockville, MD). Tissue homogenates were centrifuged at 8000 x *g* for 15 min at 4ºC and tissue supernatants were collected and stored at −80ºC.

For survival study, a subset of mice (n = 5/group) were monitored daily for 21 days for morbidity (clinical signs for infection and changes in body weight) and mortality (survival). Mice showing morbidity signs such as labored breathing, eye discharge, hunched posture and/or substantial loss of body weight (~20 to 25%), were humanely euthanized. Upon necropsy at pre-determined time points *i.e.* days 2 or 4 post infection, lung right caudal lobe was collected and fixed in 10% formalin. Fixed lung tissues were embedded in paraffin blocks and used to make 5 μm thick sections, followed by Hematoxylin and Eosin (H&E) staining for histopathology analysis evaluating tissue inflammation and pathology in a blinded manner by a board-certified veterinary pathologist.

2.18. Viral load quantitation

To determine viral titers in mouse tissue homogenates, confluent monolayers of Vero E6 cells (24-well plate format, 2×10^5 cells/well) were infected with 100 μl of ten-fold serial dilutions of mouse tissue homogenate diluted in DMEM medium for 1 h at 37 °C, 5% CO_2, with intermittent rocking every 15 min. After 1 h of viral adsorption, cells were overlaid with 800 μl of post-infection media [DMEM + 2% FBS + PSG] containing 1% low melting agar and incubated for 48 h at 37 °C, 5% CO_2. Subsequently, cells were fixed overnight with 10% formalin solution. For immunostaining, cells were washed three times with PBS and permeabilized with 0.5% Triton X-100 for 10 min at room temperature. Cells were then immuno-stained with a SARS-CoV nucleocapsid (N) protein cross-reactive monoclonal antibody (mAb, 1C7C7, Cat# ZMS1075, Sigma-Aldrich, Saint Louis, MO) diluted in 1% Bovine Serum Albumin (BSA,1 μg/ml) for 1 h at 37 °C. After incubation with the primary 1C7C7 mAb, cells were washed three times with PBS and developed with the Vectastain ABC and DAB Peroxidase Substrate kits (Vector 580 Laboratory, Inc., CA, USA) following manufacturers' instructions. Viral plaques were counted and viral titers were calculated as PFU/ml.

2.19. Statistical analysis of data

Statistical significance was determined using Prism vr. 7 Software (GraphPad Software, San Diego, CA). Unpaired, two-tailed Student's *t*-test was used for two group comparisons. Log-rank test was used to determine statistical significance of survival experiments.

3. Results and discussion

3.1. Synthesis, screening and selection of the sHA derivative

The objective of this study was to develop a potent, specific water-soluble inhibitor of the interaction between SARS-CoV-2 and human cell compatible with administration by nebulization. Sulfated polymers are already demonstrated to compete with HSPG for the binding with SARS-CoV-2 (Mycroft-West et al., 2020; Nie et al., 2021; Kwon et al., 2020). HSPG is the first human receptor involved in cell recognition by SARS-CoV-2; unfortunately, at the time of this study, no commercial kit was available to evaluate the interaction between SARS-CoV-2 S protein and HSPG. As SARS-CoV-2 S protein is expressed as homotrimer on the viral surface and to simulate a more realistic model, we performed a SARS-CoV-2 Inhibitor Screening assay by coating the plate with both the monomeric (Adipogen, US) and trimeric S protein (kindly provided by prof. A. Angelini, University of Venice). HA and Heparin were used as a negative control and selected due to their sHA-like structure.

As shown in Table 2, none of the tested polymer inhibited the interaction between SARS-CoV-2 S protein (monomer or trimer) and hACE2. A mild effect was only observed for sHA with the DS 2.1. This scaffold was selected for the next chemical optimization.

Next, HA derivatives (Table 2) were synthesized by chemical derivatization of the same sHA (DS 2.1) with different alkyl (saturated and unsaturated) and aromatic amines. The synthesis was designed to obtain a degree of derivatization of 10% mol (*vs.* sHA dimer). All compounds were successfully synthesized and purified, with a yield ranging from

Table 2
List of sulphated polymers with Degree of Sulphation (DS) expressed as the average number of sulfate groups per disaccharide repeating unit, molecular weight (MW) and the 50% inhibitory concentration (IC_{50}) of binding between the hACE2 receptor and the monomeric or trimeric forms of SARS-CoV-2 S protein. Data are expressed as mean ± S.D. of two different experiments (n = 2), both executed in triplicate. Test was validated using hACE2 blocking mAb included in kit (Adipogen, cat.AC384) showing IC_{50} of 1 μg/mL.

Scaffold	DS	Mw	IC_{50} (μg/mL) *vs* Spike protein	
		kDa	Monomer	Trimer
Heparin	2.1 ± 0.3	11 ± 1	>5000	>5000
HA	–	10 ± 1	>5000	>5000
sHA	1.3 ± 0.1	15 ± 2	4545 ± 1472	>5000
sHA	2.1 ± 0.2	17 ± 2	2587 ± 1472	5722 ± 2231

80% and 99% and with a derivatization degree ranging from 5% to 12% (mol/mol). All derivatives showed good water solubility (>8 mg/mL in PBS pH 7.0), which would be a key feature to overcome potential issues in the formulation of solution for nebulization. The sHA derivatives were tested using the same SARS-CoV-2 Inhibitor Screening kit, coated with the monomeric or trimeric SARS-CoV-2 S protein.

The sHA derivatives that showed a potent inhibitory activity in binding to S protein of SARS-COV-2 (IC_{50} < 10 μg/mL) were modified with a long alkyl chain: #**d,** #**e** and #**f** (Table 1) and their inhibitor activity against S protein monomer was comparable to each other similar to previously published studies (Toelzer et al., 2020). Other sHA derivatives with aromatic and/or bulky functional groups did not show any notable inhibitory activity. Selected inhibitors #**d**, #**e** and #**f** were tested with the same kit using the trimeric S protein of SARS-CoV-2 showing lower inhibitory potency by an order of magnitude, probably because the greater steric hi ndrance of the three subunits of the S protein shields the binding with the hydrophobic alkyl moieties of the sHA derivatives.

To evaluate the safety of these three inhibitors, a specific inhibition of hACE2 activity should be excluded. ACE2 is an enzyme responsible of the hydrolysis of angiotensin II (a vasoconstrictor peptide) into angiotensin (1–7) (a vasodilator) and inhibition of ACE2 enzymatic activity could brought to the detrimental effect of increasing blood pressure (Hamming et al., 2007). Inhibitors #**d**, #**e** and #**f** were tested using an ACE2 Activity Assay Kit Fluorometric, at the concentration of 0.8 mg/ml; all the compounds did not inhibit ACE2 (Table 1).

Further, to validate that selected inhibitors are specific to hACE2 receptor, we further investigated the inhibitory potential of these inhibitors against TMPRSS2, a transmembrane serine protease, exposed on the host cell surface involved in the priming of S protein of SARS-CoV-2 (Goc et al., 2021). TMPRSS2 is an important therapeutic target because its inhibition blocks the viral fusion with the host cell (Breining et al., 2021). Inhibitors #**d**, #**e** and #**f** tested with a TMPRSS2 Fluorogenic Assay Kit at 0.8 mg/mL showed that these do not interfere significantly with the TMPRSS2 activity (Table 1).

Among the three inhibitors, #**f** (a sHA-oleylamide derivative, Table 1) was selected as the lead compound and the cytotoxicity was evaluated in a fibroblast cell line following the ISO guidelines (Guarise et al., 2018), showing no effect on cell viability up to the concentration of 1.0 mg/ml (See SI).

3.2. *In vitro test: SPR assessment of SARS-CoV-2 S protein – sHA derivatives binding*

Binding specificity of heparin and other sulphated polysaccharides towards SARS-CoV-2 S protein is reported using SPR (Kim et al., 2020; Kwon et al., 2020; Hao et al., 2021). In this study, solutions of HA, heparin, sHA (DS 1.3 or 2.1) or **#f** were flowed for predetermined times and at different concentrations over carboxymethylated chips functionalized with either monomeric SARS-CoV-2 S protein RBD or hACE2 protein to evaluate their binging affinity. As expected, sensograms showed no interaction for HA, but, surprisingly, a similar result was

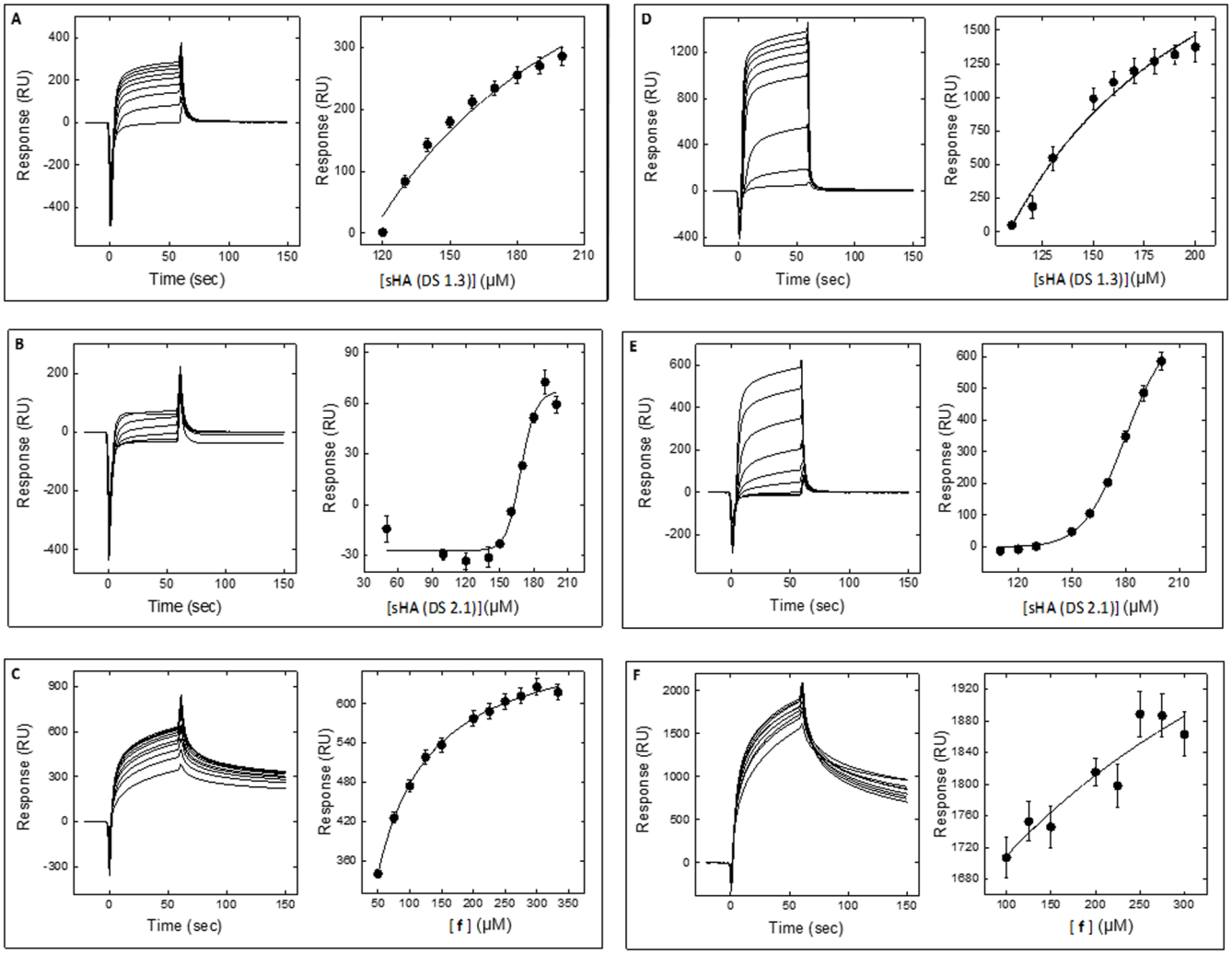

Fig. 1. Sensograms of **a)** sHA3 (DS 1.3) *vs* RBD, **b)** sHA3 (DS 2.1) *vs* RBD, **c)** #f *vs* RBD, **d)** sHA3 (DS 1.3) *vs* hACE2, **e)** sHA3 (DS 2.1) *vs* hACE2, **f)** #f *vs* hACE2.

evidenced for heparin with respect to monomeric S or hACE2 (see SI). sHA, either with DS of 1.3 or 2.1, showed fast binding and fast dissociation (identified by the sharp peak of the Fig. 1-a and **-b** *vs* monomeric SARS-CoV-2 S protein RBD, and Fig. 1-d and **-e** *vs* hACE2), while fast binding and slow dissociation towards both targets were reported for compound **#f** (see Fig. 1-c and **-f** *vs* RBD and hACE2, respectively). In Table 3, the calculated K_D values are reported for the tested polymers. These results suggest that sHA can exert a combined action by binding at the same time the viral S protein and to the hACE2.

3.3. Formulation development and preliminary stability study

sHA solutions for nebulization were developed investigating the effect of pH and terminal sterilization method on the sHA characteristic. European Pharmacopoeia indicates that solutions for nebulization must have a pH comprised between 3 and 10 (Villa-Hermosilla et al., 2022). Acidic pH is demonstrated to exert antiviral activity in ferrets (De Vries et al., 2021), while further literature assessment show how pH of medium is not critical for quick SARS-CoV-2 deactivation (Chan et al., 2020; Chin et al., 2020). Here, a sHA solution at 2.1 DS was formulated at different pH values and sterilized by filtration or by autoclave (only at pH 7.0). After 45 days of storage under accelerated stability conditions (55 °C), the MW and the residual bond sulfate were analysed and compared with the time zero values (Fig. 2). Storage in acidic solutions induced the cleavage of ester sulfate bonds, thus drastically decreasing the amount of bound sulfate and modifying the properties of the polymer. Moreover, also the MW of the polymer was strongly decreased. In buffered solution at pH 7.0, free sulfate release was reduced, and the MW was stable.

3.4. Assessment of aerosol performance

Prior being nebulized in mice, the sHA solutions (DS 2.1) at 40 mg/ml and derivative compound **#f** at 10 mg/ml was characterized (Adorni et al., 2019; Ceschan et al., 2022). The *in vitro* assessment of the nebulized solutions was performed to predict the extent of deposition in the lung of the droplets resulting from nebulization, as the total drug delivered and as the aerosol fraction having an aerodynamic diameter lower than 5 μm (Adorni et al., 2019). Table 4 illustrates the values of Drug Delivered Rate (DDR) and total Drug Delivered (DD) mean values, expressed as mg of Drug Substance delivered in the first minute and in the total of the nebulization process respectively.

Since to perform DDR and DD tests a sine pump was employed, a certain amount of the drug, corresponding to 24.2 mg, was dispersed in the environment. The volumetric output after the end of the nebulization was on average 1.1 ml, with a residual volume of solution retained by the nebulizer of 1.9 ml. This value corresponds to about a 60% and it is in line with what is normally observed with this type of device. For this reason, it could be stated that the tested solution can be efficiently aerosolized using a jet nebulizer. The DDR (%) values were similar for both the formulations (Table 4). These parameters are apparently dependent on the ampoule and the nebulizer efficiency (Rossi et al., 2018). Table 5 illustrates the values of Mass Median Aerodynamic Diameter (MMAD), Geometric Standard Deviation (GSD) and Respirable Fraction (RF%) measured for the sHA (DS 2.1) solution assessed using NGI.

As for the aerodynamic distribution profile, the sHA (DS 2.1) and the **#f** solutions had an MMAD around 3.5 μm, a value that assumes a good deposition in lungs and which led to about a 60% of the Respirable Fraction. Aerosols also exhibited a narrow distribution, with GSD values around 2.8.

Table 3
K_D values of investigated polymers towards viral monomeric S protein RBD and hACE2; n.d. = not detected.

Test Item	K_D *vs* RBD	K_D *vs* hACE2
HA	n.d.	n.d.
sHA (DS 1.3)	$4.246 \cdot 10^{-6}$	$5.047 \cdot 10^{-6}$
sHA (DS 2.1)	$3.465 \cdot 10^{-5}$	$1.936 \cdot 10^{-3}$
f	$3.583 \cdot 10^{-5}$	$6.433 \cdot 10^{-5}$
Heparin	n.d.	n.d.

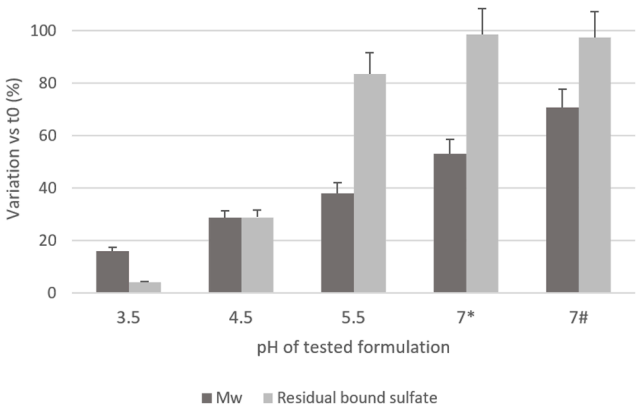

Fig. 2. sHA (Residual bound sulfate at time zero: DS 2.1 ± 0.2; Mw at time zero: 17 ± 2 k Da) stability over time in different pH and terminal sterilization method. (*) 0.2 μm filtration; (**#**) autoclave.

3.5. In vivo efficacy study in K18 hACE2 transgenic mice

The most studied SARS-CoV-2 infection animal models are transgenic mice ferrets, hamsters, and non-human primates (Lakdawala and Menachery, 2020; Muñoz-Fontela et al., 2020). The K18 hACE2 transgenic mouse model of intranasal SARS-CoV-2 infection shows the most severe clinical symptoms, comprising, but not limited to, lung viral diffusion, thrombosis, weight loss and lethality (Oladunni et al., 2020). Mice are usually infected intranasally, and SARS-CoV-2 described treatments are generally given by oral administration (Rosenke et al., 2021) or intravenous injections (Williamson et al., 2020). Administration by inhalation route (nasal or pulmonary) should be the preferred route of treatment as viral infections involves upper and lower airways. A recent study reported the treatment of SARS-CoV-2 infected animals using a nebulized antibody (Piepenbrink et al., 2021).

To determine the anti-SARS-CoV-2 efficacy of sHA and **#f** *in vivo*, we used a lethal K18-hACE2 mouse model of SARS-CoV-2 infection. Untreated (PBS) or **#f** treated SARS-CoV-2 infected mice showed a 15.9% and 18.6% body weight loss by day 4, respectively, and eventually succumbed to infection by day 5 post infection (Fig. 3A and B).

Although, sHA treated mice demonstrated a 17.9% body weight loss on day 4 post infection, these had 40% ($n = 2/5$; day 5) and 20% ($n = 1/5$; up to day 7) survival (Fig. 3A and B). Compared to SARS-CoV-2 infected PBS-treated controls, sHA treated animals infected with SARS-CoV-2 showed an increased survival time of +21%, which is close to +24% reported for a promising oral antiviral tested using the same rodent animal model (Drayman et al., 2021).

To determine the anti-SARS-CoV-2 efficacy of the sHA and **#f**, a subset of mice from each group were euthanized at days 2 ($n = 4$/group) and 4 ($n = 4$/group) post infection/post-treatment and viral load in lungs and in nasal turbinate tissue homogenates was determined by plaque assay. We detected a comparable viral load in the lungs and nasal turbinate of untreated or sHA/compound f treated mice at day 2 or 4 post infection (Fig. 4A and B).

Female K18-hACE2 mice were infected (IN) with a lethal dose (1×10^4 PFU per mouse) of SARS-CoV-2. Mice were treated with PBS or sHA (40 mg/ml) or **#f** (10 mg/ml) via aerosol twice daily in a 6–8 h interval starting 1–2 h post infection and continued up to 5 consecutive days. Mice were euthanized at 2 and 4 post infection and viral titers in lungs

Table 4
Drug Delivered Rate (DDR) and Total Drug Delivered (DD) mean values expressed as mg of API delivered upon nebulization of 3 ml of the sHA (DS 2.1) 40 mg/ml solution. [mean ± standard deviation, $n = 3$)].

	DDR (mg/min)	DD (mg)	API mg remained in nebulizer	DDR (%)	DD (%)	API mg remained in Nebulizer (%)
sHA (DS 2.1)	2.98 ± 15.10	19.72 ± 2.61	76.09 ± 0.95	2.48 ± 15.10	16.43 ± 2.61	63.41 ± 0.95
#f	0.82 ± 13.12	5.05 ± 2.76	18.25 ± 2.23	2.74 ± 13.12	16.82 ± 2.76	60.84 ± 2.23

Table 5
Mass Median Aerodynamic Diameter (MMAD), Geometric Standard Deviation (GSD), Respirable Fraction (RF <5 μm) and Respirable Dose (RD) values of the aerosol produced upon nebulization of the sHA (DS 2–1) 40 mg/ml solution (mean values ± standard deviation, $n = 3$).

	MMAD (μm)	GSD	RF <5 μm (%)	RD (mg)
sHA (DS 2.1)	3.34 ± 0.07	2.87 ± 0.14	63.0 ± 0.97	12.43 ± 0.50
#f	3.66 ± 0.14	2.80 ± 0.16	60.0 ± 2.18	3.03 ± 0.14

(**A**) and nasal turbinate (**B**) were determined by plaque assay (PFU/ml). Data represents the mean ± SEM of 4 mice in each group at each time point. Dotted lines indicate the limit of detection, LOD (10 PFU/ml). ND= Not Detected.

Similar to viral load, histopathological analysis of lungs also did not show any significant differences between the SARS-CoV-2 infected groups.

This study used a high viral inoculum (lethal dose) to test the anti-SARS-CoV-2 efficacy of sHA and **#f**, which might have outcompeted the sHA and **#f** to bind the hACE receptor. Using sub-lethal viral challenge that demonstrates a lesser clinical manifestations resulting in a mild disease onset (Dong et al., 2021) can be used to better clarify sHA and #f efficacy. Indeed, heparin, structurally similar to sHA, reduced pro-inflammatory cytokines (TNF and IL-6) in an *in vitro* model of acute lung injury (Camprubì-Rimblas et al., 2017) and is effective in reducing hypoxemia and improving the peripheral oxygen saturation in COVID-19 patients (Erelel et al., 2021).

4. Conclusions

In vitro screening of a series of HA and sHA derivatives led to the identification of inhibitors of SARS-CoV-2 S protein interaction with hACE2 receptor. *In vitro* safety of the selected compounds was verified by demonstrating the non-inhibition of hACE2 activity, fundamental to control the blood pressure in the body. The lead compounds were formulated, and stability tested at different pH values, with the aim of developing a solution for nebulization as pharmacological treatment of COVID-19. Main nebulization parameters were determined, forecasting good lung deposition. Finally, *in vivo* testing using the K18-hACE2 transgenic mouse model infected with a lethal dose of SARS-CoV-2 followed by treatment with sHA or **#f** showed that, despite a modest increase in mouse survival rate for sHA administration, this result did not translate to reduced viral titers, as well as it was not supported by histopathological evidence (data not shown). The observed increase in survival rate in the sHA treated mice was not directly associated with

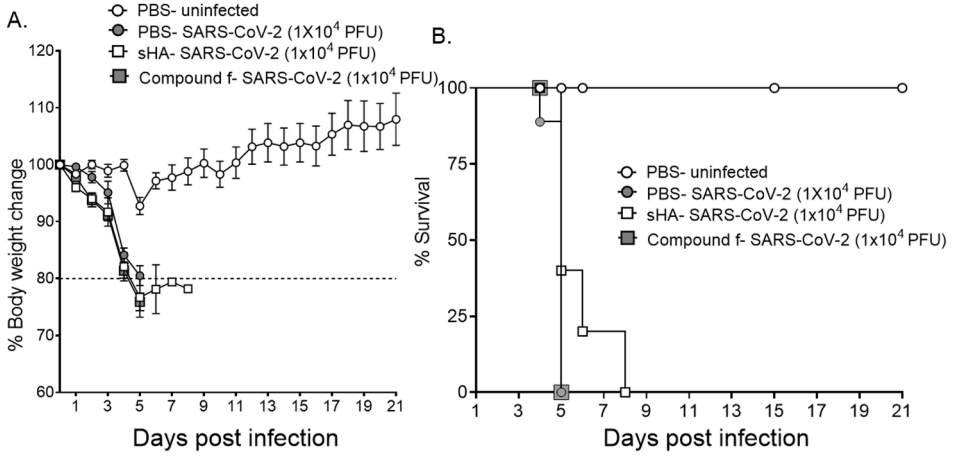

Fig. 3. Effect of aerosolized treatment of sHA and compound f on SARS-CoV-2 pathogenesis. Female K18-hACE2 mice were infected with a lethal dose (1×10^4 PFU per mouse) of SARS-CoV-2 via intranasal route. Mice were treated with PBS or sHA (40 mg/ml) or **#f** (10 mg/ml) via aerosol twice daily in a 6–8 h interval starting 1–2 h post infection and continued up to 5 consecutive days and% body weight loss (A) and survival rate (B) were monitored for 21 days. In A, Each data point represents the% body weight change (mean ±SEM) of each experimental group.

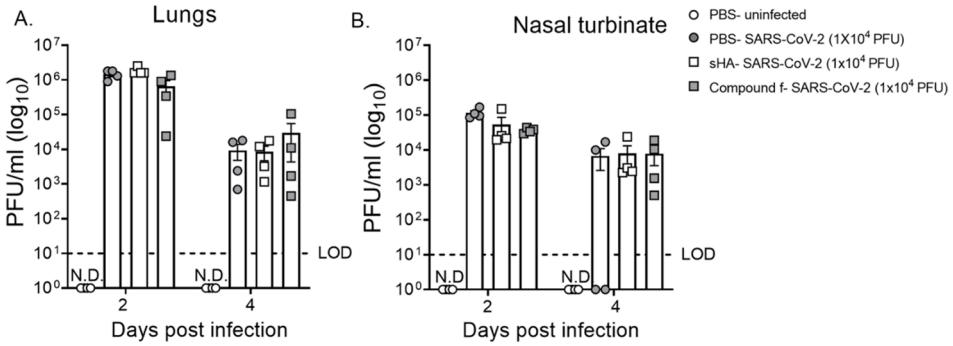

Fig. 4. sHA or compound f treatment does not lessen the viral load *in vivo*.

antiviral or anti-inflammatory effects. As a limitation, this study used a high viral inoculum, which might have outcompeted the sHA and **#f** to bind the hACE receptor. Therefore, future studies will be required to demonstrate the efficacy of sHA and/or **#f** by using sub-lethal viral challenge that demonstrates a lesser clinical manifestations resulting in a mild disease onset. Moreover, the mechanism of sHA and the possible use in acute and chronic respiratory diseases, including COVID-19 treatment, should be better clarified in terms of inflammation reduction as the likely *in vivo* mechanism in prolonging mice survival rate.

CRediT authorship contribution statement

Mauro Pavan: Conceptualization, Methodology, Investigation, Writing – original draft, Writing – review & editing. **Chiara D. Fanti:** Methodology, Investigation. **Alba Di Lucia:** Methodology, Investigation, Writing – original draft. **Elena Canato:** Methodology, Investigation. **Laura Acquasaliente:** Methodology, Investigation. **Fabio Sonvico:** Writing – review & editing. **Jennifer Delgado:** Methodology. **Amberlee Hicks:** Methodology. **Jordi B. Torrelles:** Conceptualization, Methodology, Investigation, Writing – review & editing. **Viraj Kulkarni:** Conceptualization, Methodology, Investigation, Writing – review & editing. **Varun Dwivedi:** Conceptualization, Methodology, Investigation, Writing – review & editing. **Anna M. Zanellato:** Conceptualization, Writing – review & editing. **Devis Galesso:** Conceptualization, Writing – review & editing, Supervision. **Gianfranco Pasut:** Methodology, Investigation. **Francesca Buttini:** Validation, Writing – review & editing. **Luis Martinez-Sobrido:** Conceptualization, Methodology, Investigation, Writing – review & editing. **Cristian Guarise:** Conceptualization, Methodology, Investigation, Writing – review & editing.

Data availability

The authors do not have permission to share data.

Supplementary materials

Supplementary material associated with this article can be found, in the online version, at doi:10.1016/j.ejps.2023.106489.

References

Adorni, G., Seifert, G., Buttini, F., Colombo, G., Stecanella, L.A., Krämer, I., Rossi, A., 2019. Aerosolization performance of jet nebulizers and biopharmaceutical aspects. Pharmaceutics 11 (8), 406. https://doi.org/10.3390/pharmaceutics11080406.

Alexander, D.J., Collins, C.J., Coombs, D.W., Gilkison, I.S., Hardy, C.J., Healey, G., Karantabias, G., Johnson, N., Karlsson, A., Kilgour, J.D., McDonald, P., 2008. Association of Inhalation Toxicologists (AIT) working party recommendation for standard delivered dose calculation and expression in non-clinical aerosol inhalation toxicology studies with pharmaceuticals. Inhal. Toxicol. 20 (13), 1179–1189. https://doi.org/10.1080/08958370802207318.

Bertini, S., Alekseeva, A., Elli, S., Pagani, I., Zanzoni, S., Eisele, G., Krishnan, R., Maag, K. P., Reiter, C., Lenhart, D., Gruber, R., Yates, E.A., Vicenzi, E., Naggi, A., Bisio, A., Guerrini, M., 2022. Pentosan polysulfate inhibits attachment and infection by SARS-CoV-2 in vitro: insights into structural requirements for binding. Thromb. Haemost. 122, 984–997. https://doi.org/10.1055/a-1807-0168.

Bianculli, R.H., Mase, J.D., Schulz, M.D., 2021. Antiviral polymers: past approaches and future possibilities. Macromolecules 53 (21), 9158–9186. https://doi.org/10.1021/acs.macromol.0c01273.

Breining, P., Frølund, A.L., Højen, J.F., Damsgaard Gunst, J., Staerke, N.B., Saedder, E., Cases-Thomas, M., Little, P., Nielsen, L.P., Søgaard, O.S., Kjolby, M., 2021. Camostat mesylate against SARS-CoV-2 and COVID-19—rationale, dosing and safety. Basic Clin. Pharmacol. Toxicol. 128, 204–212. https://doi.org/10.1111/bcpt.13533.

Cagno, V., Tseligka, E.D., Jones, S.T., Tapparel, C., 2019. Heparan sulfate proteoglycans and viral attachment: true receptors or adaptation bias? Viruses 11 (7), 59. https://doi.org/10.3390/v11070596.

Camprubí-Rimblas, M., Guillamat-Prats, R., Lebouvier, T., Bringué, J., Chimenti, L., Iglesias, M., Obiols, C., Tijero, J., Blanch, L., Artigas, A., 2017. Role of heparin in pulmonary cell populations in an in-vitro model of acute lung injury. Respir. Res. 18 (1), 89. https://doi.org/10.1186/s12931-017-0572-3.

Ceschan, N.E., Scioli-Montoto, S., Sbaraglini, M.L., Ruiz, M.E., Smyth, H.D.C., Bucalá, V., Ramírez-Rigo, M.V., 2022. Nebulization of a polyelectrolyte-drug system for systemic hypertension treatment. Eur. J. Pharmaceut. Sci. 170, 106108 https://doi.org/10.1016/j.ejps.2021.106108.

Chan, K.-H., Sridhar, S., Zhang, R.R., Chu, H., Fung, A.Y-F., Chan, G., Chan, J.F-W., To, K. K-W., Hung, I.F-N., Cheng, V.C-C., Yuen, K.-Y., 2020. Factors affecting stability and infectivity of SARS-CoV-2. J. Hospit. Infect. 106 (2), 226–231. https://doi.org/10.1016/j.jhin.2020.07.009.

Chin, A.W.H., Chu, J.T.S., Perera, M.R.A., Hui, K.P.Y., Yen, H.-L., Chan, M.C.W., Peiris, M., Poon, L.L.M., 2020. Stability of SARS-CoV-2 in different environmental conditions. Lancet Microbe 1 (1), e10. https://doi.org/10.1016/s2666-5247(20)30003-3.

Chu, H., Chan, J.F.W., Yuen, T.T.T., Shuai, H., Yuan, S., Wang, Y., Hu, B., Yip, C.C.Y., Tsang, J.O.L., Huang, X., Chai, Y., Yang, D., Hou, Y., Chik, K.K.H., Zhang, X., Fung, A.Y.F., Tsoi, H.W., Cai, J.P., Chan, W.M., Ip, J.D., Chu, A.W.H., Zhou, J., Lung, D.C., Kok, K.H., To, K.K.W., Tsang, O.T.Y., Chan, K.H., Yuen, K.Y., 2020. Comparative tropism, replication kinetics, and cell damage profiling of SARS-CoV-2 and SARS-CoV with implications for clinical manifestations, transmissibility, and laboratory studies of COVID-19: an observational study. Lancet Microbe 1 (1), e14–e23. https://doi.org/10.1016/S2666-5247(20)30004-5.

De Pasquale, V., Quiccione, M.S., Tafuri, S., Avallone, L., Pavone, L.M., 2021. Heparan Sulfate Proteoglycans in Viral Infection and Treatment: a Special Focus on SARS-CoV-2. Int. J. Mol. Sci. 22 (12), 6574. https://doi.org/10.3390/ijms22126574.

De Vries, R.D., Schmitz, K.S., Bovier, F.T., Predella, C., Khao, J., Noack, D., Haagmans, B. L., Herfst, S., Stearns, K.N., Drew-Bear, J., Biswas, S., Rockx, B., McGill, G., Dorrello, N.V., Gellman, S.H., Alabi, C.A., De Swart, R.L., Moscona, A., Porotto, M., 2021. Intranasal fusion inhibitory lipopeptide prevents direct-contact SARS-CoV-2 transmission in ferrets. Science 371 (6536), 1379–1382. https://doi.org/10.1126/science.abf4896.

Dong, W., Mead, H., Tian, L., Park, J.G., Garcia, J.I., Jaramillo, S., Barr, T., Kollath, D.S., Coyne, V.K., Stone, N.E., Jones, A., Zhang, J., Li, A., Wang, L.S., Milanes-Yearsley, M., Torrelles, J.B., Martinez-Sobrido, L., Keim, P.S., Barker, B.M., Caligiuri, M.A., Yu, J., 2021. The K18-Human ACE2 transgenic mouse model recapitulates non-severe and severe COVID-19 in response to an infectious dose of the SARS-CoV-2 virus. J. Virol. 96 (1), e0096421 https://doi.org/10.1128/JVI.00964-21.

Drayman, N., DeMarco, J.K., Jones, K.A., Azizi, S.A., Froggatt, H.M., Tan, K., Maltseva, N.I., Chen, S., Nicolaescu, V., Dvorkin, S., Furlong, K., Kathayat, R.S., Firpo, M.R., Mastrodomenico, V., Bruce, E.A., Schmidt, M.M., Jedrzejczak, R., Muñoz-Alía, M.Á., Schuster, B., Nair, V., Han, K.Y., O'Brien, A., Tomatsidou, A., Meyer, B., Vignuzzi, M., Missiakas, D., Botten, J.W., Brooke, C.B., Lee, H., Baker, S. C., Mounce, B.C., Heaton, N.S., Severson, W.E., Palmer, K.E., Dickinson, B.C., Joachimiak, A., Randall, G., Tay, S., 2021. Masitinib is a broad coronavirus 3CL inhibitor that blocks replication of SARS-CoV-2. Science 373 (6557), 931–936. https://doi.org/10.1126/science.abg5827.

Erelel, M., Kaskal, M., Akbal-Dagistan, O., Issever, H., Dagistanli, A.S., Balkanci, H., Oguz, M.S., Qarayeva, A., Culha, M., Erturk, A., Basarir, N.S., Sahin, G., Uresin, A.Y., Araman, A.O., Medetalibeyoglu, A., Tukek, T., Oncul, M.O., Yildiz-Pekoz, A., 2021. Early effects of low molecular weight heparin therapy with soft-mist inhaler for COVID-19-induced hypoxemia: a phase IIb trial. Pharmaceutics 13 (11), 1768. https://doi.org/10.3390/pharmaceutics13111768.

Farinholt, T., Doddapaneni, H., Qin, X., Menon, V., Meng, Q., Metcalf, G., Chao, H., Gingras, M.C., Avadhanula, V., Farinholt, P., Agrawal, C., Muzny, D.M., Pierda, P.A., Gibbs, R.A., Petrosino, J., 2021. Transmission event of SARS-CoV-2 delta variant reveals multiple vaccine breakthrough infections. BMC Med. 19 (255) https://doi.org/10.1186/s12916-021-02103-4.

Goc, A., Niedzwiecki, A., Rath, M., 2021. Polyunsaturated ω-3 fatty acids inhibit ACE2-controlled SARS-CoV-2 binding and cellular entry. Sci. Rep. 11, 5207 https://doi.org/10.1038/s41598-021-84850-1.

Guarise, C., Barbera, C., Pavan, M., Pluda, S., Celestre, M., Galesso, D., 2018. Dopamine-functionalized sulphated hyaluronic acid as a titanium implant coating enhances biofilm prevention and promotes osseointegration. Biofouling 34 (7), 719–730. https://doi.org/10.1080/08927014.2018.1491555.

Hamming, I., Cooper, M., Haagmans, B., Hooper, N., Korstanje, R., Osterhaus, A., Timens, W., Turner, A., Navis, G., Van Goor, H., 2007. The emerging role of ACE2 in physiology and disease. J. Pathol. 212, 1–11. https://doi.org/10.1002/path.2162.

Hao, W., Ma, B., Li, Z., Wang, X., Gao, X., Li, Y., Qin, B., Shang, S., Cui, S., Tan, Z., 2021. Binding of the SARS-CoV-2 spike protein to glycans. Sci. Bull. 66 (12), 1205–1214. https://doi.org/10.1016/j.scib.2021.01.010.

Hintze, V., Miron, A., Moeller, S., Schnabelrauch, M., Wiesmann, H.P., Worch, H., Scharnweber, D., 2012. Sulfated hyaluronan and chondroitin sulfate derivatives interact differently with human transforming growth factor-β1 (TGF-β1). Acta Biomater. 8 (6), 2144–2152. https://doi.org/10.1016/j.actbio.2012.03.021.

Inglis, T.J.J., Mathee, K., 2021. JMM Profile: severe acute respiratory syndrome coronavirus 2 (SARS-CoV-2). J. Med. Microbiol. 70 (3) https://doi.org/10.1099/jmm.0.001336.

Kim, S.Y., Jin, W., Sood, A., Montgomery, D.W., Grant, O.C., Fuster, M.M., Fu, L., Dordick, J.S., Woods, R.J., Zhang, F., Linhardt, R.J., 2020. Characterization of heparin and severe acute respiratory syndrome-related coronavirus 2 (SARS-CoV-2) spike glycoprotein binding interactions. Antivir. Res. 181, 104873 https://doi.org/10.1016/j.antiviral.2020.104873.

Kwon, P.S., Oh, H., Kwon, S.J., Jin, W., Zhang, F., Fraser, K., Hong, J.J., Linhardt, R.J., Dordick, J.S., 2020. Sulfated polysaccharides effectively inhibit SARS-CoV-2 *in vitro*. Cell Discov. 6 (50) https://doi.org/10.1038/s41421-020-00192-8.

Lakdawala, S.S., Menachery, V.D., 2020. The search for a COVID-19 animal model. Science 368 (6494), 942–943. https://doi.org/10.1126/science.abc6141.

Lamers, M.M., Haagmans, B.L., 2022. SARS-CoV-2 pathogenesis. Nat. Rev. Microbiol. 20, 270–284. https://doi.org/10.1038/s41579-022-00713-0.

Möller, S., Theiß, J., Deinert, T.I.L., Golat, K., Heinze, J., Niemeyer, D., Wyrwa, R., Schnabelrauch, M., Bogner, E., 2022. High-sulfated glycosaminoglycans prevent coronavirus replication. Viruses 14 (2), 413. https://doi.org/10.3390/v14020413.

Muñoz-Fontela, C., Dowling, W.E., Funnell, S.G.P., Gsell, P.S., Riveros-Balta, A.X., Albrecht, R.A., Andersen, H., Baric, R.S., Carroll, M.W., Cavaleri, M., Qin, C., Crozier, I., Dallmeier, K., de Waal, L., de Wit, E., Delang, L., Dohm, E., Duprex, W.P., Falzarano, D., Finch, C.L., Frieman, M.B., Graham, B.S., Gralinski, L.E., Guilfoyle, K., Haagmans, B.L., Hamilton, G.A., Hartman, A.L., Herfst, S., Kaptein, S.J.F., Klimstra, W.B., Knezevic, I., Krause, P.R., Kuhn, J.H., Le Grand, R., Lewis, M.G., Liu, W.-C., Maisonnasse, P., McElroy, A.K., Munster, V., Oreshkova, N., Rasmussen, A.L., Rocha-Pereira, J., Rockx, B., Rodríguez, E., Rogers, T.F., Salguero, F.J., Schotsaert, M., Stittelaar, K.J., Thibaut, H.J., Tseng, C.-T., Vergara-Alert, J., Beer, M., Brasel, T., Chan, J.F.W., García-Sastre, A., Neyts, J., Perlman, S., Reed, D.S., Richt, J.A., Roy, C.J., Segalés, J., Vasan, S.S., Henao-Restrepo, A.M., Barouch, D.H., 2020. Animal models for COVID-19. Nature 586, 509–515. https://doi.org/10.1038/s41586-020-2787-6.

Mycroft-West, C.J., Su, D., Pagani, I., Rudd, T.R., Elli, S., Gandhi, N.S., Guimond, S.E., Miller, G.J., Meneghetti, M.C.Z., Nader, H.B., Li, Y., Nunes, Q.M., Procter, P., Mancini, N., Clementi, M., Bisio, A., Forsyth, N.R., Ferro, V., Turnbull, J.E., Guerrini, M., Fernig, D.G., Vicenzi, E., Yates, E.A., Lima, M.A., Skidmore, M.A., 2020. Heparin inhibits cellular invasion by SARS-CoV-2: structural dependence of the interaction of the spike S1 receptor-binding domain with heparin. Thromb. Haemost. 120 (12), 1700–1715. https://doi.org/10.1055/s-0040-1721319.

Nie, C., Pouyan, P., Lauster, D., Trimpert, J., Kerkhoff, Y., Szekeres, G.P., Wallert, M., Block, S., Sahoo, A.K., Dernedde, J., Pagel, K., Kaufer, B.B., Netz, R.R., Ballauff, M., Haag, R., 2021. Polysulfates block SARS-CoV-2 uptake through electrostatic interactions. Angew. Chem. Int. Ed. 60 (15870) https://doi.org/10.1002/anie.202102717.

Oladunni, F.S., Park, J.G., Pino, P.A., Gonzalez, O., Akhter, A., Allué-Guardia, A., Olmo-Fontánez, A., Gautam, S., Garcia-Vilanova, A., Ye, C., Chiem, K., Headley, C., Dwivedi, V., Parodi, L.M., Alfson, K.J., Staples, H.M., Schami, A., Garcia, J.I., Whigham, A., Platt, R.N., Gazi, M., Martinez, J., Chuba, C., Earley, S., Rodriguez, O. H., Mdaki, S.D., Kavelish, K.N., Escalona, R., Hallam, C.R.A., Christie, C., Patterson, J.L., Anderson, T.J.C., Carrion, R.Jr, Dick, E.J.Jr, Hall-Ursone, S., Schlesinger, L.S., Alvarez, X., Kaushal, D., Giavedoni, L.D., Turner, J., Martinez-Sobrido, L., Torrelles, J.B., 2020. Lethality of SARS-CoV-2 infection in K18 human angiotensin-converting enzyme 2 transgenic mice. Nat. Commun. 11 (1), 6122. https://doi.org/10.1038/s41467-020-19891-7.

Paiardi, G., Richter, S., Oreste, P., Urbinati, C., Rusnati, M., Wade, R.C., 2022. The binding of heparin to spike glycoprotein inhibits SARS-CoV-2 infection by three mechanisms. J. Biolog. Chem. 298 (2), 101507 https://doi.org/10.1016/j.jbc.2021.101507.

Pavan, M., Beninatto, R., Galesso, D., Panfilo, S., Vaccaro, S., Messina, L., Guarise, C., 2016. A new potential spreading factor: streptomyces koganeiensis hyaluronidase. A comparative study with bovine testes hyaluronidase and recombinant human hyaluronidase of the HA degradation in ECM. Biochimica et Biophysica Acta (BBA) - Gener. Subj. 1860 (4), 661–668. https://doi.org/10.1016/j.bbagen.2015.12.024.

Piepenbrink, M.S., Park, J.G., Oladunni, F.S., Deshpande, A., Basu, M., Sarkar, S., Loos, A., Woo, J., Lovalenti, P., Sloan, D., Ye, C., Chiem, K., Bates, C.W., Burch, R.E., Erdmann, N.B., Goepfert, P.A., Truong, V.L., Walter, M.R., Martinez-Sobrido, L., Kobie, J.J., 2021. Therapeutic activity of an inhaled potent SARS-CoV-2 neutralizing human monoclonal antibody in hamsters. Cell Rep. Med. 2 (3), 100218 https://doi.org/10.1016/j.xcrm.2021.100218.

Rosenke, K., Hansen, F., Schwarz, B., Feldmann, F., Haddock, E., Rosenke, R., Barbian, K., Meade-White, K., Okumura, A., Leventhal, S., Hawman, D.W., Ricotta, E., Bosio, C.M., Martens, C., Saturday, G., Feldmann, H., Jarvis, M.A., 2021. Orally delivered MK-4482 inhibits SARS-CoV-2 replication in the Syrian hamster model. Nat. Commun. 12 (1), 2295. https://doi.org/10.1038/s41467-021-22580-8.

Rossi, I., Sonvico, F., McConville, J.T., Rossi, F., Fröhlich, E., Zellnitz, S., Rossi, A., Del Favero, E., Bettini, R., Buttini, F., 2018. Nebulized coenzyme Q10 nanosuspensions: a versatile approach for pulmonary antioxidant therapy. Eur. J. Pharmaceut. Sci. 113, 159–170. https://doi.org/10.1016/j.ejps.2017.10.024.

Tay, M.Z., Poh, C.M., Rénia, L., MacAry, P.A., Ng, L.F.P., 2020. The trinity of COVID-19: immunity, inflammation and intervention. Nat. Rev. Immunol. 20, 363–374. https://doi.org/10.1038/s41577-020-0311-8.

Toelzer, C., Gupta, K., Yadav, S.K.N., Borucu, U., Davidson, A.D., Williamson, M.K., Shoemark, D.K., Garzoni, F., Staufer, O., Milligan, R., Capin, J., Mulholland, A.J., Spatz, J., Fitzgerald, D., Berger, I., Schaffitzel, C., 2020. Free fatty acid binding pocket in the locked structure of SARS-CoV-2 spike protein. Science (6517), 370. https://doi.org/10.1126/science.abd3255.

Tregoning, J.S., Flight, K.E., Higham, S.L., Wang, Z., Pierce, B.F., 2021. Progress of the COVID-19 vaccine effort: viruses, vaccines and variants *versus* efficacy, effectiveness and escape. Nat. Rev. Immunol. 21, 626–636. https://doi.org/10.1038/s41577-021-00592-1.

Trypsteen, W., Van Cleemput, J., Van Snippenberg, W., Gerlo, S., Vandekerckhove, L., 2020. On the whereabouts of SARS-CoV-2 in the human body: a systematic review. PLoS Pathog. 16 (10), e1009037 https://doi.org/10.1371/journal.ppat.1009037.

Villa-Hermosilla, M.-C., Negro, S., Barcia, E., Hurtado, C., Montejo, C., Alonso, M., Fernandez-Carballido, A., 2022. Celecoxib microparticles for inhalation in COVID-19-related acute respiratory distress syndrome. Pharmaceutics 14, 1392. https://doi.org/10.3390/pharmaceutics14071392.

WHO Coronavirus (COVID-19) Dashboard, https://covid19.who.int/.

Williamson, B.N., Feldmann, F., Schwarz, B., Meade-White, K., Porter, D.P., Schulz, J., van Doremalen, N., Leighton, I., Yinda, C.K., Pérez-Pérez, L., Okumura, A., Lovaglio, J., Hanley, P.W., Saturday, G., Bosio, C.M., Anzick, S., Barbian, K., Cihlar, T., Martens, C., Scott, D.P., Munster, V.J., de Wit, E., 2020. Clinical benefit of remdesivir in rhesus macaques infected with SARS-CoV-2. Nature 585 (7824), 273–276. https://doi.org/10.1038/s41586-020-2423-5.

Wolff, R.K., 2015. Toxicology Studies for Inhaled and Nasal Delivery. Mol. Pharm. 12 (8), 2688–2696. https://doi.org/10.1021/acs.molpharmaceut.5b00146, 2015.

Wu, D., Koganti, R., Lambe, U.P., Yadavalli, T., Nandi, S.S., Shukla, D., 2020. Vaccines and therapies in development for SARS-CoV-2 infections. J. Clin. Med. 9 (6), 1885. https://doi.org/10.3390/jcm9061885.